PolyEnergetics
Clean, safe, reliable nuclear energy

WHITE PAPER · MULTIPHYSICS

Validation of a Moltres Multiphysics Model of the Molten Salt Reactor Experiment (MSRE)

POLYENERGETICS PRIVATE LIMITED

VERSION 1.0

KEYWORDS

Molten Salt Reactor Experiment, MSRE, Moltres, MOOSE, Multiphysics, Delayed Neutron Precursors, Neutron Diffusion, Thermal Hydraulics, PolyEnergetics

Abstract

The Molten Salt Reactor Experiment (MSRE) is simulated with Moltres, an open-source MOOSE-based application that couples multigroup neutron diffusion, delayed neutron precursor (DNP) transport with advection, and separate energy equations for the flowing fuel salt and the stationary graphite moderator. A two-dimensional axisymmetric model of the core, using two neutron energy groups and six precursor groups with Serpent-generated temperature-dependent cross sections, is solved as a single Jacobian-Free Newton–Krylov system and benchmarked against the original ORNL MSRE design calculations. The neutron energy flux magnitudes, the shapes of the axial temperature profiles, the fuel–graphite temperature difference and the peak power density (34.2 against 31 kW l^{-1} in the MSRE) are acceptably reproduced, while the fast neutron energy flux is underpredicted by 15 %, an effect of considering the fast and epithermal range into a single group. The axial peak positions of the six precursor fields are set by the interplay between the precursor half-life period and the precursor advection. The circulating-fuel effective delayed neutron fraction of 369 pcm agrees to within 2 % of the MSRE reference value of 362 pcm, corresponding to a 47 % reduction from the static value of 696 pcm through precursor advection. Gamma heating in the graphite, at 7.5 % of fission power, is the sole mechanism producing the moderator hotter than fuel inversion characteristic of graphite-moderated MSRs.

RESULTS AT A GLANCE

369 pcm

Circulating-fuel effective delayed neutron fraction, within 2 % of the 362 pcm MSRE reference

–47 %

Reduction from the static value of 696 pcm through precursor advection

34.2 kW/l

Peak power density, against 31 kW/l in the MSRE design report

992.2 K

Peak graphite temperature with gamma heating (Γ = 0.075), against a 971.4 K fuel peak

READER'S NOTE

In a molten salt reactor the fuel is dissolved in the coolant and flows through the core, so neutron physics, the drift of delayed neutron precursors and heat transport all depend on one another. This paper solves those coupled equations together in Moltres for a two-dimensional model of the MSRE core, operated at Oak Ridge National Laboratory from 1965 to 1969, and compares the results with the original ORNL design calculations. pcm is a unit of reactivity equal to one hundred-thousandth of a change in the neutron multiplication factor.

CONTENTS

1. Introduction

Molten salt reactors (MSRs) is Generation IV reactor concept in which the nuclear fuel is dissolved directly in a circulating molten salt coolant rather than being contained within solid fuel elements [1]. This configuration offers several potential advantages over conventional solid-fuelled reactors, including operation at low pressure and high temperature, substantial margins to coolant boiling, and the potential for continuous fuel processing and fission-product removal. Because the fuel and coolant occupy the same fluid phase, the neutronic and thermal-hydraulic behaviour of an MSR is fundamentally different from that of conventional reactors. In particular, the continuous movement of fissile material and delayed neutron precursors (DNPs) introduces an additional transport mechanism that directly affects reactor kinetics and feedback. Neutronics, precursor transport and thermal hydraulics are therefore coupled at the level of the governing equations and must solve them together.

The Molten Salt Reactor Experiment (MSRE), operated at Oak Ridge National Laboratory between 1965 and 1969, remains the only graphite-moderated, thermal-spectrum MSR for which design calculations and measured data exists [2, 3]. It is a benchmark experimental case for modern MSR codes.

Moltres is an open-source MSR simulation application built on the MOOSE finite-element framework and developed by the Advanced Reactors and Fuel Cycles group at the University of Illinois [4]. It solves the time-dependent multigroup neutron diffusion equations coupled to a set of DNP transport equations that carry an advection term, and separate energy equations for the flowing fuel and the stationary moderator. Its physics is assembled from individual MOOSE kernels, each contributing one term of the governing equation, and the number of neutron energy groups and the precursor groups is given as input. Lindsay et al. [5] introduced Moltres and demonstrated its coupled neutronics and thermal hydraulics capability on 2-D axisymmetric and 3-D MSRE models, obtaining neutron flux and temperature distributions in qualitative agreement with the ORNL design calculations. Pater [6] used Moltres for a more detailed MSRE study and compared the results with ORNL experimental data. Later, Park [7] extended this work in two ways. First, verified the loop delayed neutron precursor drift model in Moltres for the MSRE zero-power pump start-up and coast-down transients. Second, developed a hybrid S_N diffusion method for control-rod modelling and validated it on a 3-D MSRE model against OpenMC and measured MSRE rod-worth and rod-drop data. Shi and Fratoni [8] used GeN-Foam to simulate the complete MSRE fuel loop in 2-D, including the core, lower and upper plena, downcomer and external loop, and implemented an adjoint solver to benchmark effective delayed neutron fraction. Two steady-state calculations i.e. static and fuel flowing at 1200 gpm are performed and predicted effective delayed neutron fraction and compared the results with ORNL MSRE reports.

The present work is simulation of the two-dimensional axisymmetric MSRE core in Moltres, benchmarked simultaneously against the original ORNL MSRE design calculations [2, 3]. The steady-state neutron flux distributions, the six-group DNP concentration fields, the power density and the coupled fuel–graphite temperature fields are examined, and the influence of gamma heating in the moderator is isolated by a dedicated comparison with the corresponding kernel disabled.

2. Mathematical model

2.1 Neutronics

Neutrons are described by the time-dependent multigroup diffusion equations. For each energy group g [6],

$$\frac{1}{v_g}\frac{\partial \phi_g}{\partial t} - \nabla \cdot D_g \nabla \phi_g + \Sigma_g^r \phi_g = \sum_{g' \neq g}^{G} \Sigma_{g' \to g}^s \phi_{g'} + \chi_g^p \sum_{g'=1}^{G} (1-\beta)\, \nu_{g'} \Sigma_{g'}^f \phi_{g'} + \chi_g^d \sum_{i}^{I} \lambda_i C_i \tag{1}$$

where ϕ_g is the scalar flux of group g, v_g the group neutron speed, D_g the group diffusion coefficient and $\Sigma^r{}_g$ the macroscopic cross section for removal of neutrons from group g. The right-hand side terms include the in-scattering from all other groups, the prompt fission source distributed over the prompt spectrum $\chi^p{}_g$, and the delayed fission source distributed over the delayed spectrum $\chi^d{}_g$. Here $\nu_{g'}$ is the number of neutrons released per fission induced by group g', $\Sigma^f{}_{g'}$ the corresponding macroscopic fission cross section, β the delayed neutron fraction, G the number of energy groups and I the number of precursor groups.

2.2 Delayed neutron precursors

The concentration C_i of the i-th precursor group obeys [6],

$$\frac{\partial C_i}{\partial t} = \sum_{g'=1}^{G} \beta_i \, \nu_{g'} \Sigma_{g'}^{f} \phi_{g'} - \lambda_i C_i - \frac{\partial}{\partial z} (u \, C_i) \tag{2}$$

with β_i the delayed neutron fraction and λ_i the decay constant of group *i*. The first two terms on the right hand side are the production and decay terms of a static-fuel reactor. The third term is what distinguishes a liquid-fuelled system: it is the advection of precursors with the salt, written here for the axial direction only, since the fuel in the present model moves upward through straight channels. It is this term that displaces the delayed source towards the core outlet, removes part of it from the active region altogether, and reduces β_i below its static value.

2.2.1 Static delayed neutron fraction

In a stationary-fuel reactor every precursor decays where it is born, so the delayed neutron fraction is the tabulated value averaged over the fuel region. It is evaluated here as an unweighted volume average of the temperature-dependent cross-section data over the fuel salt within the active core [9, 10],

$$\beta_{\text{static}} = \frac{1}{V_f} \int_{V_f} \beta\big(T(\mathbf{r})\big) \, dV = \frac{1}{V_f} \int_{V_f} \sum_{i=1}^{6} \beta_i\big(T(\mathbf{r})\big) \, dV \tag{3}$$

This quantity carries no information about the transport of precursors by the flowing salt, and is therefore referred to throughout as the static delayed neutron fraction.

2.2.2 Delayed and total neutron sources

When the fuel circulates, a fraction of the precursors generated in the core is carried into the external loop before decaying, so the associated delayed neutrons are not emitted within the active region. The delayed neutron source retained in the core follows from the steady-state precursor field [9, 10],

$$S_d = \sum_{i=1}^{6} \lambda_i \int_{V_f} C_i \, dV \tag{4}$$

The corresponding total neutron production within the core, comprising the prompt fission source and the delayed source [9, 10],

$$S_{\text{tot}} = \int_{V_f} \left[(1-\beta) \sum_{g=1}^{G} \nu \Sigma_{f,g}\, \phi_g + \sum_{i=1}^{6} \lambda_i C_i \right] dV \tag{5}$$

2.2.3 Circulating-fuel effective delayed neutron fraction

The effective delayed neutron fraction under circulation is defined as the ratio of delayed to total neutrons born within the active core [9, 10],

$$\beta_{\text{eff}}^{\text{circ}} = \frac{S_d}{S_{\text{tot}}} = \frac{\sum_{i=1}^{6} \lambda_i \int_{V_f} C_i\, dV}{\int_{V_f} \left[(1-\beta) \sum_{g=1}^{G} \nu \Sigma_{f,g}\, \phi_g + \sum_{i=1}^{6} \lambda_i C_i \right] dV} \tag{6}$$

Both numerator and denominator are unweighted volume integrals, so this quantity represents the fraction of neutrons produced in the core that are delayed.

2.3 Energy conservation

The fuel salt temperature T_f is governed by an advection–diffusion equation with a volumetric fission source [6],

$$\rho_f c_{p,f} \frac{\partial T_f}{\partial t} + \nabla \cdot (\rho_f c_{p,f}\, \mathbf{u}\, T_f - k_f \nabla T_f) = Q_f \tag{7}$$

$$Q_f = \sum_{g=1}^{G} \epsilon_{f,g}\, \Sigma_{f,g}\, \phi_g \tag{8}$$

where ρ_f, $c_{p,f}$ and k_f are the density, specific heat capacity and thermal conductivity of the fuel salt, u its velocity, $\epsilon_{f,g}$ the energy released per fission by group g neutrons and $\Sigma_{f,g}$ macroscopic fission cross-section in group g.

The graphite moderator is stationary, so its energy equation retains conduction only [6],

$$\rho_m c_{p,m} \frac{\partial T_m}{\partial t} + \nabla \cdot (-k_m \nabla T_m) = Q_m \tag{9}$$

The moderator source term Q_m represents heat deposited in the graphite by gamma rays and by neutron and beta irradiation. Because the mean free path of the gammas is long compared with the channel pitch, this deposition is nearly proportional to the core-average fission heat rather than to the local one, and is modelled as [6],

$$Q_m = \frac{1}{V_{\text{core}}} \gamma \int_{\text{core}} Q_f \, dV \tag{10}$$

with V_{core} the core volume and γ the gamma heating fraction. Following Pater [6], the spatial shape of the deposition is imposed through

$$\gamma = \Gamma \frac{\pi^2}{4} \cos\left(\frac{\pi r}{2R}\right) \sin\left(\frac{\pi z}{H}\right) \tag{11}$$

where R and H are the core radius and height and Γ is the user-specified fraction of total fission power deposited in the moderator. In the MSRE this fraction was measured to lie between 6 and 8 %, and Γ = 0.075 is adopted here.

The equations above are discretised with continuous Galerkin finite elements on a single mesh and solved as one coupled nonlinear system by the Jacobian-Free Newton–Krylov method provided by MOOSE, so that the neutronic, precursor and thermal fields are converged simultaneously at every time step rather than exchanged between separate solvers.

2.4 Model setup

The computational domain is a two-dimensional axisymmetric (r, z) representation of the MSRE core, adopted from Pater [6], with a radius of 73 cm and a height of 162.56 cm. The core comprises 14 thin fuel channels interleaved with 14 thicker graphite regions, yielding a fuel volume fraction of 0.225, consistent with the MSRE design (Figure 1).

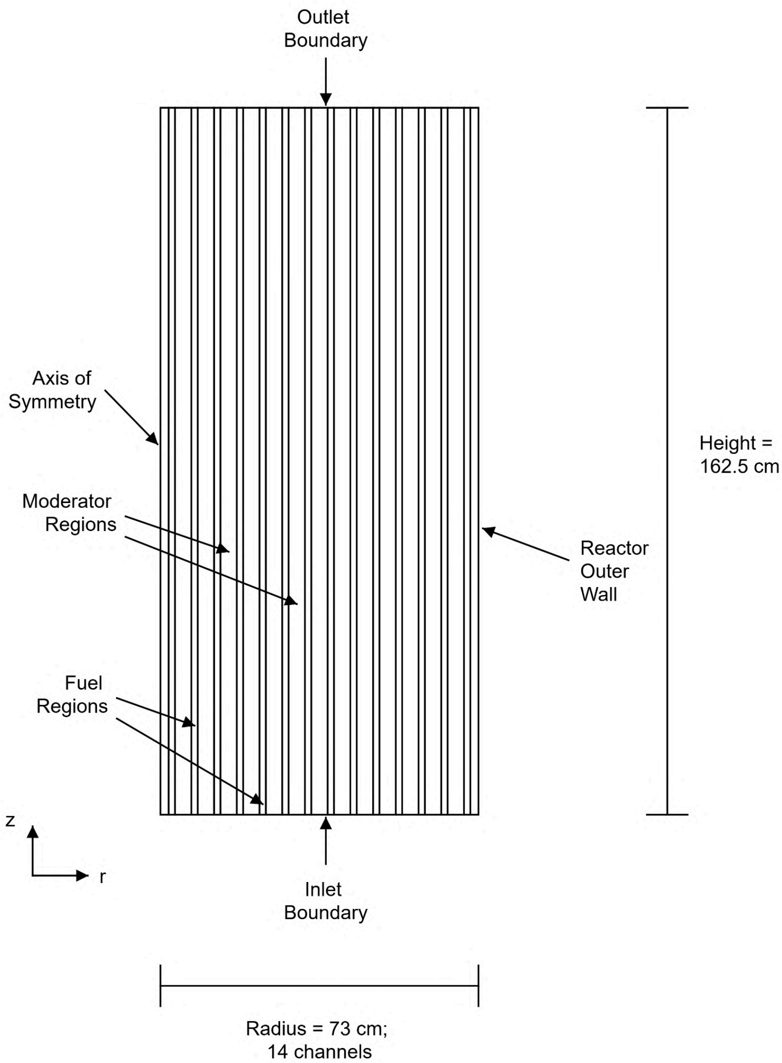

Figure 1. Schematic of the MSR model geometry.

The left boundary is the axis of symmetry; the fuel enters at the bottom and leaves at the top. Vacuum boundary conditions are applied to the neutron flux on the top, bottom and outer radial surfaces. The thermal loop is closed without meshing the primary heat exchanger. The core inlet plane and the outer radial wall are assigned a temperature that tracks the instantaneous area-averaged outlet core temperature minus 27.8 K. This is based on the consideration that the heat exchanger removes the full thermal power each timestep, fixing the core temperature rise at its nominal MSRE value. Two-group cross sections (group boundary at 0.78 eV) were generated with

Serpent 2 from a three-dimensional MSRE model and homogenized separately for the fuel salt and the graphite. The constants are tabulated at eleven temperatures from 633 K to 1600 K and spline-interpolated by Moltres as the coupled solution evolves, with the six precursor decay constants taken from Pater, with decay constants of 0.01, 0.03, 0.12, 0.30, 0.85 and 2.85 s^{-1}.

TABLE 1. PRINCIPAL SIMULATION INPUT PARAMETERS [6]

SR.	PARAMETER	VALUE	UNIT
1	Fuel flow speed	0.217	$m\ s^{-1}$
2	Initial temperature	922	K
3	Core temperature rise	27.8	K
4	Gamma heating fraction Γ	0.075	–
5	Number of neutron groups	2	–
6	Number of DNP groups	6	–
7	Fuel thermal conductivity	5.53	$W\ m^{-1}\ K^{-1}$
8	Fuel specific heat capacity	1967	$J\ kg^{-1}\ K^{-1}$
9	Fuel density	$2.146 \exp[-2.124 \times 10^{-4} (T - 922)]$	$g\ cm^{-3}$
10	Graphite thermal conductivity	31.2	$W\ m^{-1}\ K^{-1}$
11	Graphite specific heat capacity	1760	$J\ kg^{-1}\ K^{-1}$
12	Graphite density	$1.86 \exp[-1.8 \times 10^{-5} (T - 922)]$	$g\ cm^{-3}$
13	Core radius R / height H	73 / 162.56	cm
14	Fuel volume fraction	0.225	–

3. Results and discussion

3.1 Approach to the steady state

The simulation is started from a uniform initial temperature of 922 K with the reactor power stepped instantaneously from zero to full, and simulations are continued until the coupled fields cease to change. The initial transients and the approach to the steady state is shown in Figure 2. The y-axis on the left gives the average core outlet temperature, core inlet temperature and average temperature of the fuel and moderator. The right y-axis i.e. flux ratio represents the ratio of group 1 flux at current time step to group 1 flux at previous time step.

At initial times, the fast flux grows, peaking in growth rate at t ≈ 2 s and reaching maximum power at t ≈ 8 s where the ratio crosses unity. Negative fuel-temperature feedback then drives the flux into a shallow decay before it moves to unity beyond ~40 s, indicating a stationary critical state. Core outlet and average fuel temperatures lag the flux peak by roughly 10 s, turning over at t ≈ 18 - 20 s once heat removal balances production. The graphite moderator responds far more slowly and is still rising at 60 s, reaching above the mean fuel temperature and is expected, as the gamma heating of the moderator is considered.

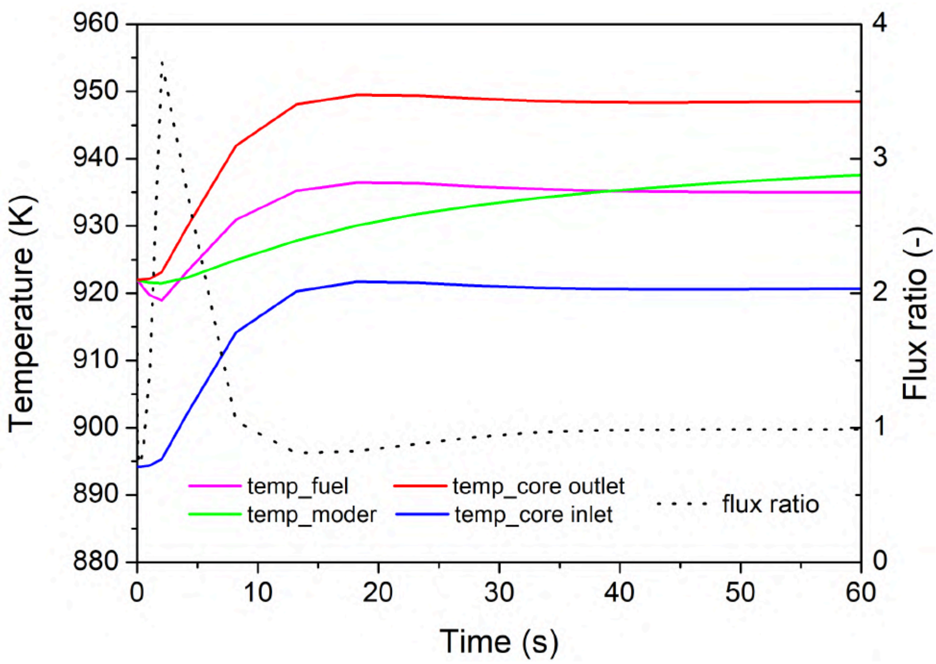

Figure 2. Evolution of the core outlet, area-averaged fuel and area-averaged moderator temperatures, together with the flux ratio, during the approach to the nominal steady state.

3.2 Neutron flux distributions

The fast neutron energy group ϕ_1 and thermal neutron energy group ϕ_2 show the expected flux distribution produced by vacuum boundary conditions on all three outer surfaces, with the maximum value at the geometric midplane as shown in Figure 3(a) and (b). The peak fast flux is 1.2 × 10^{14} cm^{-2} s^{-1} and the peak thermal flux 4.5 × 10^{13} cm^{-2} s^{-1}, a ratio close to three that follows directly from all neutrons being born fast while only a fraction survive to be thermal.

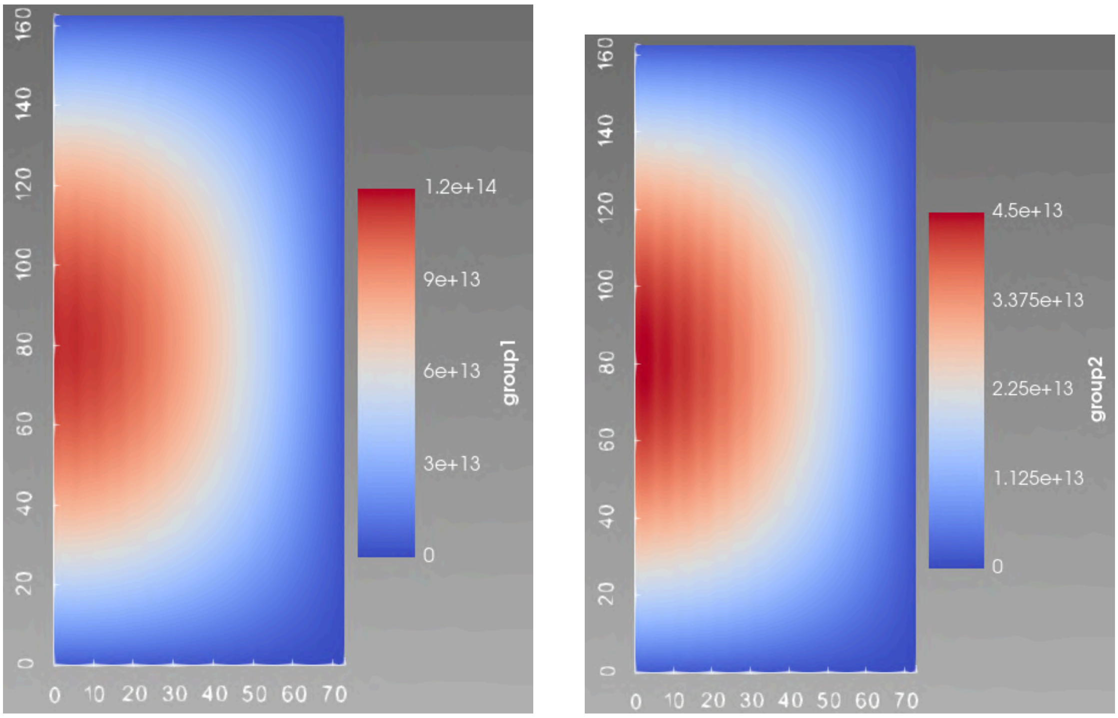

(A) (B)

Figure 3. Steady-state neutron flux in the two-dimensional axisymmetric model: (a) fast group (group - 1) and (b) thermal group (group - 2), in cm^{-2} s^{-1}.

The channel structure is resolved in both fields but is far more pronounced in the thermal group, where the vertical striations of Figure 3(b) mark the graphite regions in which neutrons slow down and accumulate. The fast group shows the complementary pattern, with local maxima in the fuel channels where fission occurs.

Figure 4 is the quantitative core of the neutronics benchmark. Against the ORNL design calculations [2, 3], the thermal flux agrees well in magnitude, but the shapes differ near the axis: the design report shows a depression in the central 15 cm, rising from 3.2 × 10^{13} at r = 0 to a maximum of 4.1 × 10^{13} cm^{-2} s^{-1} near $r \approx$ 20 cm, whereas the present model peaks on the axis. The cause is geometric — the control rod thimbles occupy the centre of the real core and absorb thermal neutrons there, and they are not represented in the two-dimensional model.

The fast flux, by contrast, is uniformly underpredicted by roughly 20 % on the radial profile (1.15 × 10^{14} against 1.45 × 10^{14} cm^{-2} s^{-1} on the axis) and by about 15 % on the axial profile (1.16 × 10^{14} against 1.37 × 10^{14} cm^{-2} s^{-1} at the peak). The consideration of two-group diffusion treatment of the MSRE against a 32-group design calculation [5]: collapsing the entire fast and epithermal range into a single group with a temperature-interpolated diffusion coefficient cannot represent the spectral detail that governs fast-group leakage, and the two-group model responds by depressing the fast flux. The axial profiles shows the geometric difference visible as well: the ORNL curves extend beyond z = 0 and z = 162.56 cm because the design model included the upper and lower plena and reflector, while the present model terminates at the active core boundary with a vacuum condition.

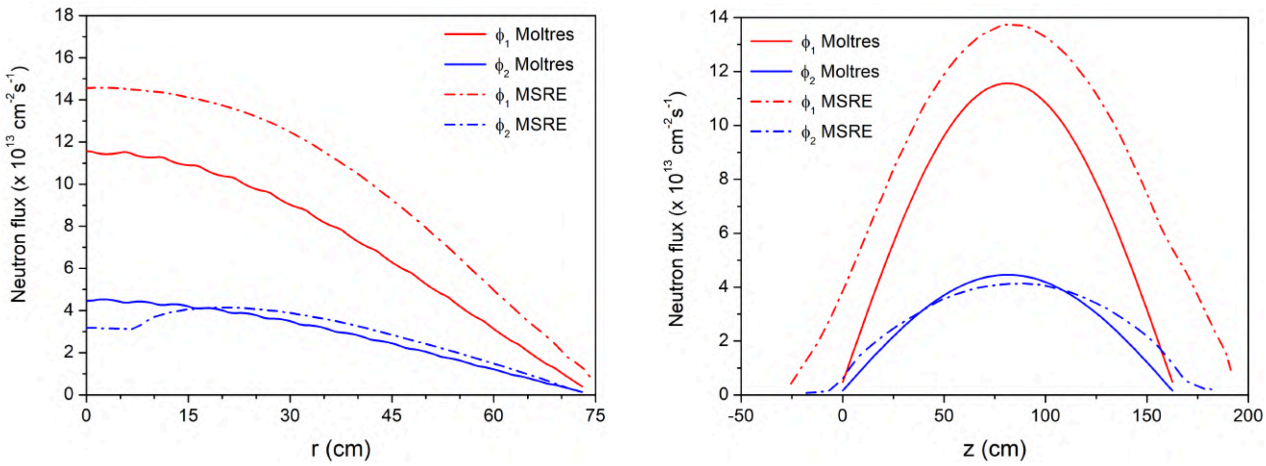

(A) (B)

Figure 4. Fast and thermal flux profiles from the present simulation compared with the ORNL MSRE design report: (a) radial profiles at the core midplane, (b) axial profiles along the core centre line.

The consistency of the discrepancy across two independent Moltres models is the useful result here. It means the fast-flux deficit can be attributed to the physics approximation with some confidence, and it identifies the number of energy groups as the first thing to change if closer agreement with the design data is required.

3.3 Delayed neutron precursor distributions

The precursor fields are where the liquid-fuel character of the reactor becomes most apparent, and is shown in Figure 5. In Figure 5(a), at the midplane, all six groups fall off monotonically with r, following the fission source that produces them; the ordering of the curves reflects the group delayed fractions β_i, with group 4 dominant at 1.37 × 10^{10} cm^{-3} on the axis, followed by groups 2 and 3, and group 6 lowest at 2.5 × 10^{8} cm^{-3}.

The axial distribution of Figure 5(b) is a direct measurement of the precursor advection term. Every group is essentially zero at the inlet, because fresh salt entering the core carries no precursors in this model, and each then builds up along the channel. Where each group peaks is set by the competition between its decay constant and the transit time: at 0.217 m s^{-1} the salt spends about 7.5 s traversing the 1.63 m core, so a group with $\lambda_i \gg 1/7.5\ s^{-1}$ decays as fast as it is produced and tracks the local flux, while a group with $\lambda_i \ll 1/7.5\ s^{-1}$ simply accumulates.

Group 6, i.e., shortest lived precursor, with $\lambda_6 = 2.85\ s^{-1}$ and a mean life of 0.35 s, therefore shows maximum near the core midplane, in phase with the fission source. Group 4 ($\lambda_4 = 0.30\ s^{-1}$) peaks at $1.8 \times 10^{10}\ cm^{-3}$ around $z \approx 125$ cm, well above the flux maximum. Groups 2 and 1, with mean lives of 33 s and 100 s against a 7.5 s transit, are still rising when the salt leaves the core at $z = 162.56$ cm, reaching 1.32×10^{10} and $2.7 \times 10^{9}\ cm^{-3}$ respectively.

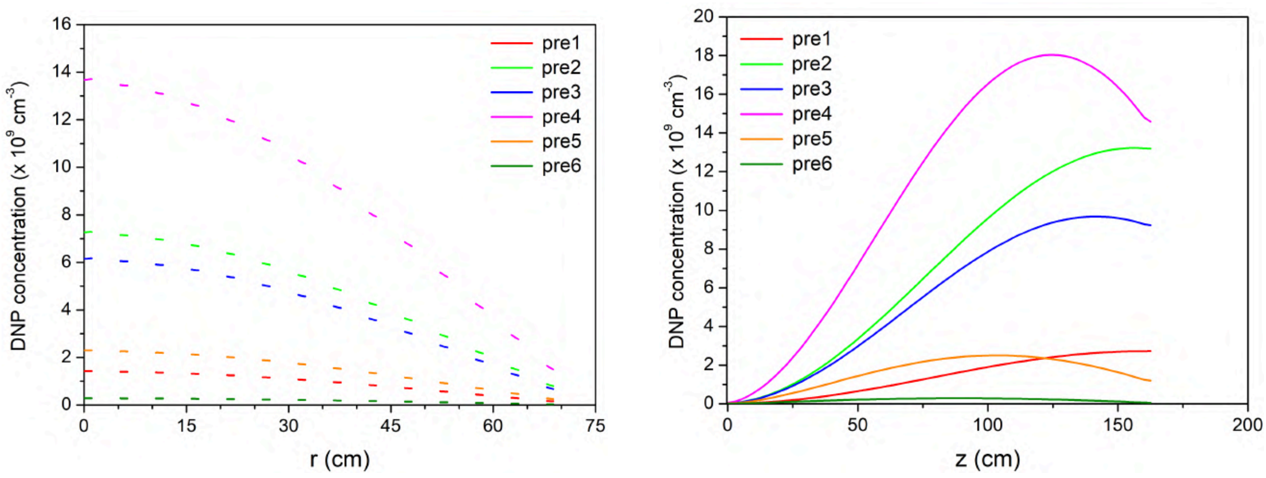

(A) (B)

Figure 5. Steady-state concentrations of the six delayed neutron precursor groups: (a) radial distribution at the core midplane, (b) axial distribution along fuel channel 1.

Figure 6 shows the concentration fields for the longest lived and shortest lived precursor groups.

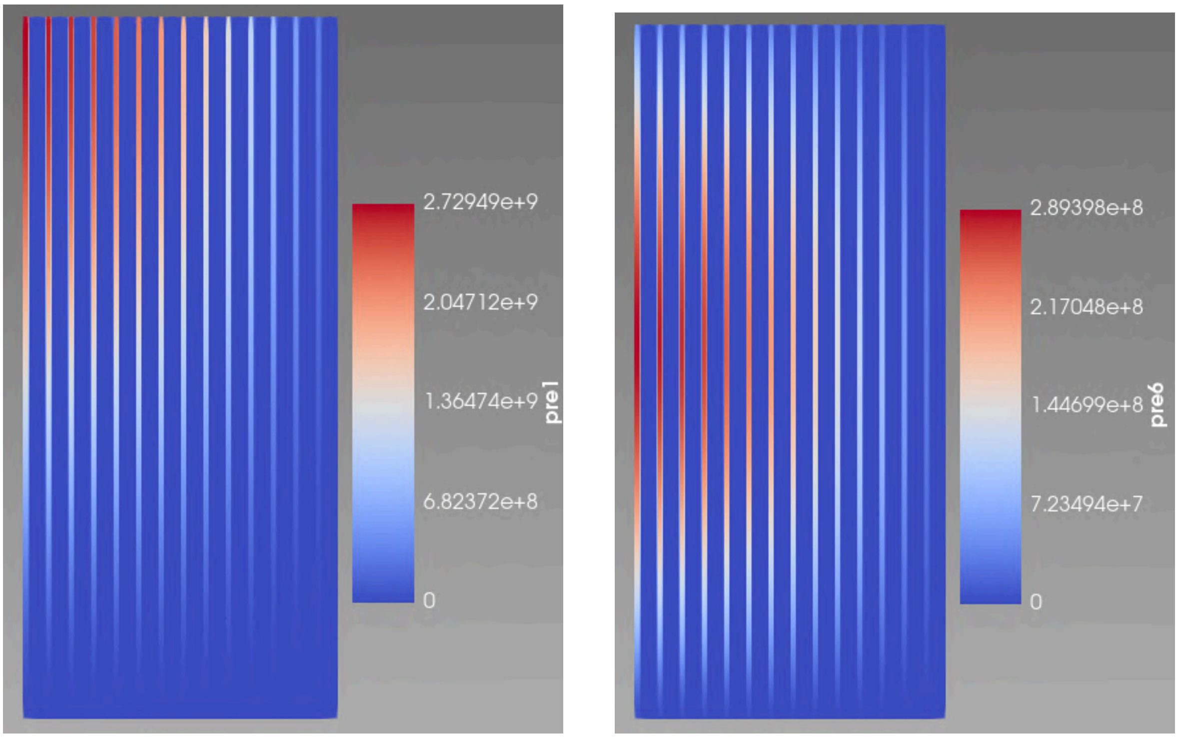

(A) (B)

Figure 6. Two-dimensional concentration fields of (a) longest-lived precursor group (Group -1 λ_1 = 0.01 s^{-1}, and (b) the shortest-lived group (Group-6), λ_6 = 2.85 s^{-1}, in cm^{-3}.

Both fields are confined strictly to the fuel channels — the precursors exist only in the salt, so the graphite regions appear as gaps — and both decrease with radius as the fission source does. The difference between the two -groups appears in the axial direction. The shortest-lived group is concentrated around the core mid-height, closely following the flux, with a maximum of 2.89×10^8 cm^{-3}. The longest-lived group, at 2.73×10^9 cm^{-3}, is advected upward towards the outlet, having been carried there faster before it decays.

3.4 Power density and temperature fields

The power density distribution, shown in Figure 7(a), follows the shape of the fast flux (Figure 3(a)) and is confined to the fuel channels. The predicted peak power density is 34.2 kW/l, compared with 31 kW/l reported in the MSRE design report [2]. This overprediction of roughly 10% is consistent with the omission of the control rod thimbles from the model, which concentrates the power within a slightly smaller effective volume.

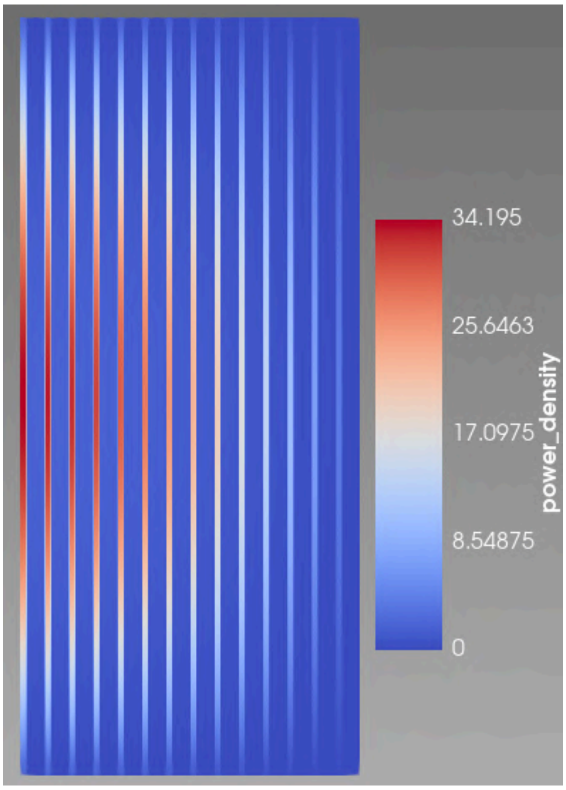

(A)

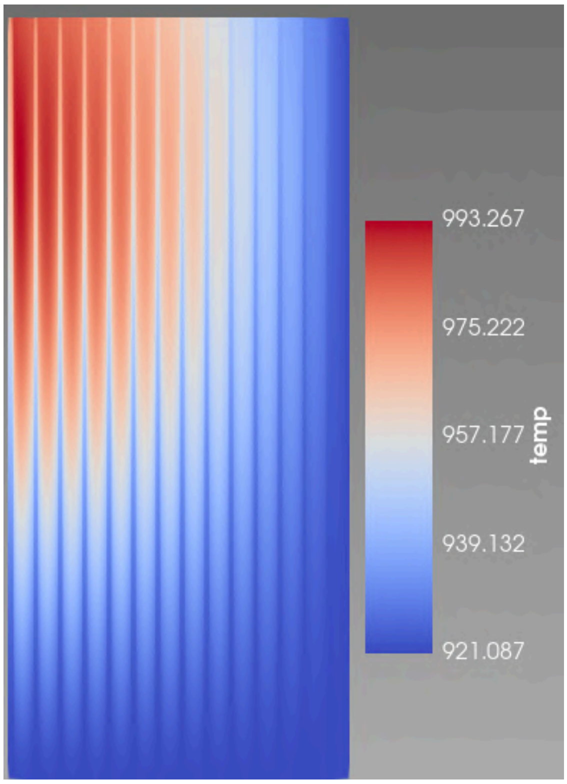

(B)

Figure 7. Steady-state (a) power density in kW l^{-1} and (b) temperature in K.

The temperature field of Figure 7(b) spans 921.1 to 993.3 K and shows two features simultaneously. The first is the axial rise driven by advection: the hottest material is near the top of the core, not at the maximum power region, because the salt integrates the heat it receives as it travels upward. Also, the hottest material is graphite rather than fuel. In a solid-fuelled reactor the fuel is necessarily hotter than the coolant; here the salt is the coolant, it is continuously renewed, and it removes its own fission heat directly, whereas the stationary graphite can shed the gamma energy deposited in it only by conduction into the adjacent salt. The moderator therefore runs hotter than the fuel, an inversion that is characteristic of graphite-moderated MSRs and was observed in the MSR experiments.

The radial profiles of Figure 8(a) resolve the channel structure clearly. The inlet profile is flat at 921 K, as imposed by the boundary condition. At the midplane and the outlet the temperature decreases with radius, following the power distribution, and is strongly modulated: the maxima are the graphite regions, heated by gamma, and the minima the fuel channels, from which heat is advected away. The modulation amplitude is largest near the axis, where the power density is greatest, and collapses towards r = 73 cm where the outer wall boundary condition holds the temperature at the inlet value. The outlet profile falls from 988 K on the axis to 921 K at the wall, a radial spread of 67 K across the core that is considerably larger than the 27.8 K mean rise between inlet and outlet and which is a direct consequence of the unflattened radial power profile.

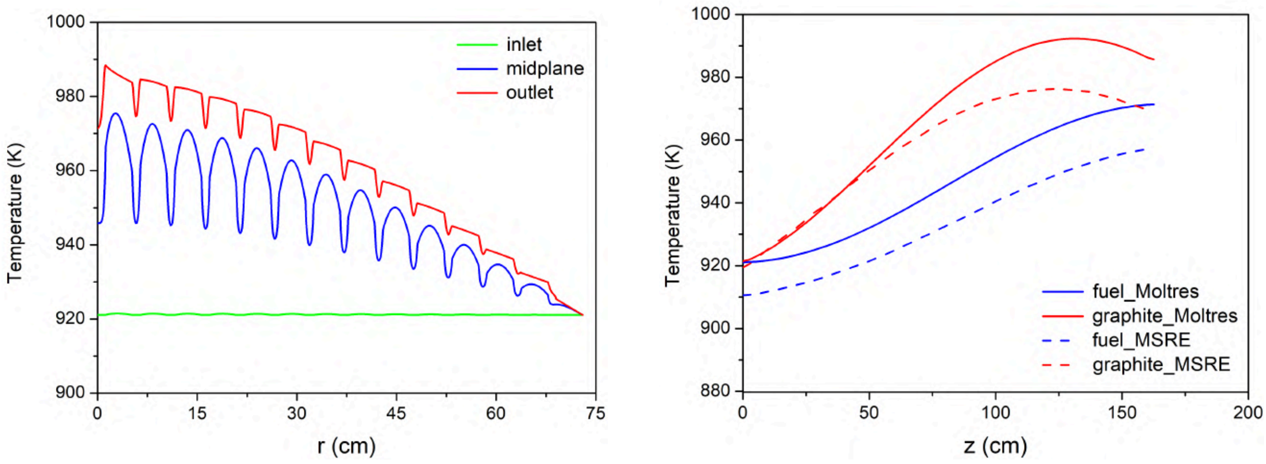

(A) (B)

Figure 8. Temperature profiles: (a) radial profiles at the core inlet, midplane and outlet from the present simulation, and (b) axial profiles in the hottest fuel channel and the adjacent graphite compared with the MSRE design calculations.

Figure 8(b) compares the axial profiles in the hottest channel with the ORNL design calculations [2]. The shapes agree well. The fuel temperature rises monotonically with the characteristic S-profile produced by integrating a cosine-like power distribution in the flow direction (Figure 7(a)). The graphite temperature rises faster in the lower half of the core, reaching a maximum of 992.2 K at z =130 cm above the midplane, because the fuel that cools it is hotter there — and then falls slightly towards the outlet as the local power drops.

3.5 Effective delayed neutron fraction for circulating fuel

In the present model, the Serpent-generated group-constant data gives the static value as, β_{static} = 696 pcm [6]. As the fuel salt circulates, delayed neutron precursors are carried out of the active core before they decay, so a fraction of the delayed neutrons is emitted in the external loop instead of in the core. This advection of precursors reduces the effective delayed neutron fraction $\beta^{circ}{}_{eff}$ from its static value β_{static}. For the MSRE, the reference value under circulating conditions is 362 pcm [6], and the present Moltres simulation gives 369 pcm at the final steady state — a difference of 2%. The reduction relative to the static value of 696 pcm therefore amounts to 327 pcm, or 47% of the delayed neutrons lost to precursor advection.

3.6 Effect of gamma heating in the moderator

As the gamma heating (Equations 10 and 11) is the mechanism responsible for the fuel–moderator temperature inversion, the model was rerun with the corresponding kernel disabled and the total power held fixed. Figure 9 shows this effect.

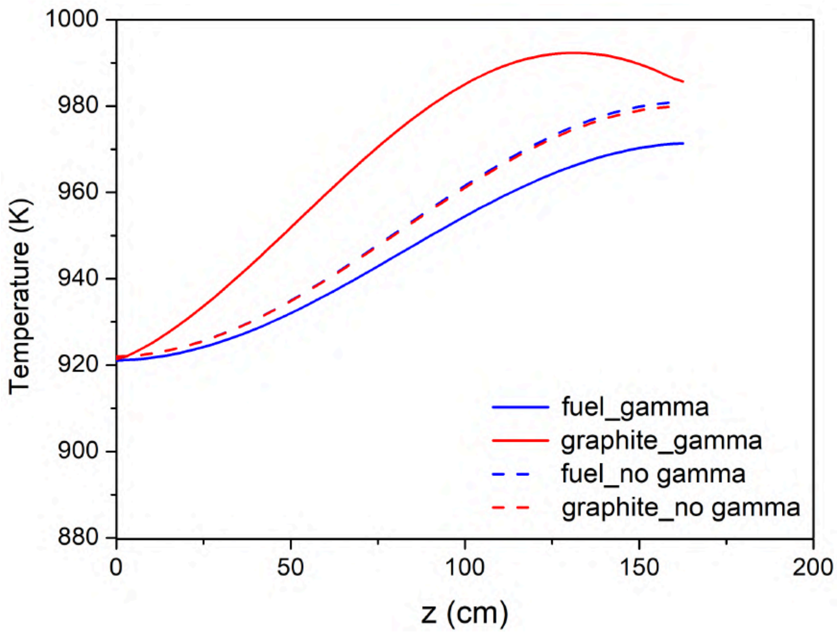

Figure 9. Axial temperature distributions in the hottest fuel channel and adjacent graphite, with and without the gamma heating kernel active.

Without gamma heating the fuel and graphite curves collapse onto one another: they are separated by less than about 1 K over the entire core height, ending at 981.0 and 979.9 K respectively at the outlet. This is the expected outcome, since the only remaining heat source in the graphite is the conduction heat transfer, and the graphite can then be no hotter than the fluid heating it. With gamma heating active, the graphite peak rises to 992.2 K while the fuel peak temperature falls to 971.4 K at the core outlet.

4. Conclusions

The two-dimensional axisymmetric MSRE core model was reconstructed and simulated in Moltres, and its predictions were compared with the original ORNL design calculations.

The model agrees well with the ORNL design calculations qualitatively, although the quantitative agreement is mixed. The thermal flux magnitudes, the shapes of the axial temperature profiles, the fuel–graphite temperature difference and the peak power density are all reproduced satisfactorily. The fast flux, however, is underpredicted by 15–20%. This discrepancy is likely attributable mainly to the two-group energy treatment: merging the fast and epithermal ranges into a single group with a temperature-interpolated diffusion coefficient cannot capture the spectral detail that governs fast-neutron leakage. The omission of the control rods and their thimbles from the model may also contribute, since it alters the local neutron balance near the core centre and hence the shape of the fast flux profile.

The model reproduces the behaviour that distinguishes a circulating-fuel core. The relative magnitudes of the six precursor fields follow the group delayed fractions, while their axial peak positions are set by the interplay between decay and transport: groups with half life period short against the 7.5 s core transit remain in phase with the fission source, and the longer-lived groups are displaced towards, or carried beyond, the outlet. Gamma heating in the graphite produces the moderator hotter than fuel, which collapses to nearly 1 K difference once the kernel is disabled.

Three limitations apply to these results. First, the external loop is not modelled, so precursor re-entry is neglected and the loss of the longest-lived groups is overestimated. Second, the omission of the control rod thimbles causes the neutron group 1 and 2 flux values discrepancy and part of the power density overprediction. Third, the gamma heating fraction is an input parameter, constrained by measurement only to 6–8%.

Nomenclature

C_i	Concentration of delayed neutron precursor group i (cm^{-3})
$c_{p,f}$	Specific heat capacity of fuel salt ($J\ kg^{-1}\ K^{-1}$)
$c_{p,m}$	Specific heat capacity of graphite moderator ($J\ kg^{-1}\ K^{-1}$)
D_g	Diffusion coefficient of energy group g (cm)
G	Number of neutron energy groups ($G = 2$)
H	Active core height (cm)
I	Number of delayed neutron precursor groups ($I = 6$)
k_f	Thermal conductivity of fuel salt ($W\ m^{-1}\ K^{-1}$)
k_m	Thermal conductivity of graphite moderator ($W\ m^{-1}\ K^{-1}$)
Q_f	Volumetric fission heat source in fuel salt ($W\ m^{-3}$)
Q_m	Volumetric heat source in graphite moderator ($W\ m^{-3}$)
R	Core radius (cm)
r	Radial coordinate (cm)
$\mathbf{r}$	Position vector (cm)
S_d	Delayed neutron source retained within the active core (s^{-1})
S_{tot}	Total (prompt + delayed) neutron production within the active core (s^{-1})
T	Temperature (K)
T_f	Fuel salt temperature (K)
T_m	Graphite moderator temperature (K)
t	Time (s)
u	Axial fuel salt velocity ($m\ s^{-1}$)
V_{core}	Active core volume (cm^3)
V_f	Fuel salt volume within the active core (cm^3)
v_g	Neutron speed in energy group g ($cm\ s^{-1}$)
z	Axial coordinate (cm)

Greek symbols

β	Total delayed neutron fraction (pcm)
β_i	Delayed neutron fraction of precursor group i (pcm)
β_{static}	Static delayed neutron fraction, Eq. (3) (pcm)

β^{circ}_{eff}	Circulating-fuel effective delayed neutron fraction, Eq. (6) (pcm)
Γ	Fraction of total fission power deposited in the moderator
γ	Spatial gamma heating distribution factor, Eq. (11)
$\varepsilon_{f,g}$	Energy released per fission induced by group-g neutrons (J)
λ_i	Decay constant of precursor group i (s^{-1})
ν_g	Mean number of neutrons released per fission induced by group g
ρ_f	Fuel salt density (kg m^{-3})
ρ_m	Graphite moderator density (kg m^{-3})
$\Sigma_{f,g}$	Macroscopic fission cross section of group g (cm^{-1})
$\Sigma_{r,g}$	Macroscopic removal cross section of group g (cm^{-1})
$\Sigma_{s,g'\rightarrow g}$	Macroscopic scattering cross section from group g' to g (cm^{-1})
Φ_g	Scalar neutron flux of group g (cm^{-2} s^{-1})
$\chi_{p,g}$	Fraction of prompt fission neutrons born in group g
$\chi_{d,g}$	Fraction of delayed neutrons born in group g

Subscripts and superscripts

circ	Circulating fuel
core	Active core
d	Delayed
eff	Effective
f	Fuel salt (on ρ, c_p, k, T, Q, V); fission (on Σ, ε)
g, g'	Neutron energy group indices
i	Precursor group index
m	Graphite moderator
p	Prompt
r	Removal
s	Scattering
static	Stationary fuel
tot	Total

References

[1] J. Serp, M. Allibert, O. Beneš, S. Delpech, O. Feynberg, V. Ghetta, D. Heuer, D. Holcomb, V. Ignatiev, J. L. Kloosterman, L. Luzzi, E. Merle-Lucotte, J. Uhlíř, R. Yoshioka, D. Zhimin, "The molten salt reactor (MSR) in generation IV: Overview and perspectives," *Progress in Nuclear Energy*, 77 (2014) 308–319.

[2] R. C. Robertson, "MSRE Design and Operations Report, Part I: Description of Reactor Design," ORNL-TM-728, Oak Ridge National Laboratory, 1965.

[3] P. Haubenreich and J. Engel, "Experience with the Molten-Salt Reactor Experiment," Nuclear Applications & Technology, vol. 8, pp. 118-136, February 1970.

[4] A. Lindsay, Moltres, software for simulating Molten Salt Reactors, University of Illinois at Urbana-Champaign, 2017. [Online]. Available: https://github.com/arfc/moltres

[5] A. Lindsay, G. Ridley, A. Rykhlevskii, K. Huff, "Introduction to Moltres: An application for simulation of Molten Salt Reactors," *Annals of Nuclear Energy*, **114**, 530–540, 2018.

[6] M. Pater, "Multiphysics simulations of Molten Salt Reactors using the Moltres code," MSc thesis, Université Paris-Saclay / Seaborg Technologies, 2019.

[7] S. M. Park, "Advancements in Moltres for time-dependent multiphysics molten salt reactor modeling," PhD dissertation, University of Illinois Urbana-Champaign, Urbana, IL, 2025.

[8] J. Shi, M. Fratoni, "GeN-Foam model and benchmark of delayed neutron precursor drift in the Molten Salt Reactor Experiment," EPJ Web of Conferences, 247, 06040, 2021 (PHYSOR2020).

[9] Mattioda, P. Ravetto, and G. Ritter, "Effective Delayed Neutron Fraction for Fluid-fuel Systems," *Annals of Nuclear Energy* **27**(16), pp. 1523-1532 (2000).

[10] M. Aufiero, et al., "Calculating the Effective Delayed Neutron Fraction in the Molten Salt Fast Reactor: Analytical, Deterministic and Monte Carlo Approaches," *Annals of Nuclear Energy* **65**, pp. 78-90 (2014).